

Controlled Polymerization and Self-Assembly of Halogen-Bridged Diruthenium Complexes in Organic Media and Their Dielectrophoretic Alignment

Rempei Kuwahara,^{†,‡} Shigenori Fujikawa,^{‡,§,¶} Keita Kuroiwa,^{‡,⊥} and Nobuo Kimizuka*,^{†,‡}

[†]Department of Chemistry and Biochemistry, Graduate School of Engineering, International Research Center for Molecular Systems (IRCMS), Kyushu University, 744 Moto-oka, Nishi-ku, Fukuoka 819-0395, Japan

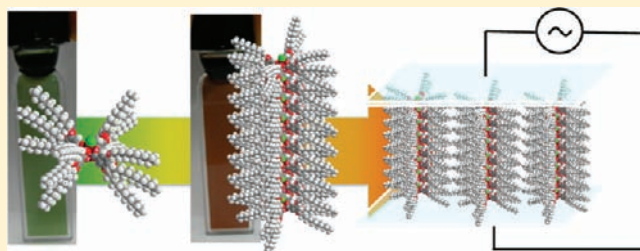
[‡]JST, CREST, 744 Moto-oka, Nishi-ku, Fukuoka 819-0395, Japan

[§]Innovative Nanopatterning Research Laboratory, RIKEN, 2-1, Hirosawa, Wako, Saitama 351-0198, Japan

[⊥]Department of Nanoscience, Faculty of Engineering, Sojo University, 4-22-1 Ikeda, Kumamoto 860-0082, Japan

Supporting Information

ABSTRACT: Lipophilic paddlewheel biruthenium complexes $[\text{Ru}_2(\mu\text{-O}_2\text{CR})_3\text{X}]_n$ ($\text{O}_2\text{CR} = 3,4,5\text{-tridodecyloxybenzoate}$, $\text{X} = \text{Cl, I}$) self-assemble in organic media to form halogen-bridged coordination polymers. The polymerization is accompanied by spectral changes in $\pi(\text{RuO}_2\text{Ru}_2) \rightarrow \pi^*(\text{Ru}_2)$ and $\pi(\text{axial ligand}) \rightarrow \pi^*(\text{Ru}_2)$ absorption bands. These polymeric complexes form lyotropic liquid crystals in *n*-decane at concentrations above ~ 100 unit mM. The bridging halogen axial ligands ($\text{X} = \text{Cl or I}$) exert significant influences on their electronic structures and self-assembling characteristics: the chloride-bridged polymers give hexagonally aligned ordered columnar structure (columnar hexagonal phase, Col_{h}), whereas the iodide-bridged polymers form less ordered columnar nematic (Col_{n}) phase, as revealed by small-angle X-ray diffraction measurements. Chloro-bridged coordination polymers dispersed in *n*-decane are thermally intact even at the elevated temperature of 70 °C. In contrast, iodo-bridged polymers show reversible dissociation and reassembly phenomena depending on temperature. These halogen-bridged coordination polymers show unidirectional alignment upon applying alternating current (ac) electric field as investigated by crossed polarizing optical microscopy and scanning electron microscopy. The unidirectionally oriented columns of chloro-bridged polymers are accumulated upon repetitive application of the ac voltage, whereas iodo-bridged coordination polymers show faster and reversible alignment changes in response to turning on-and-off the electric field. The controlled self-assembly of electronically conjugated linear complexes provide a potential platform to design electric field-responsive nanomaterials.



INTRODUCTION

Formation of electronically conjugated molecular wires via self-assembly of component molecules and their controlled alignment in between electrodes are among priority challenges in nanochemistry.¹ A feasible solution to simultaneously pursue these issues would be to develop electronically conjugated coordination polymers based on the self-assembly of metal ions and bridging ligands, and further to control their orientation in response to the applied electronic field. Pseudo-one-dimensional (1D) metal complexes are promising candidates as such self-assembling nanowires, because they show wide variety of electronic structures which are controllable depending on the constituent metal ions and bridging ligands.^{2–5} However, they usually exist as basic structural motifs of crystalline solid, and accordingly their characterization have been the subject of research in solid-state chemistry. The ability to disperse these 1D complexes in solution and to control their electronic structures, macroscopic orientation between electrodes are essential to develop future neuromorphic devices, which

spontaneously self-assemble into nanocircuits. We have devised a supramolecular methodology to convert crystalline quasi-1D halogen-bridged mixed valence complexes $[\text{Pt}(\text{en})_2][\text{Pt}(\text{en})_2\text{X}_2]^{4+}$ (en ; ethylenediamine, X ; Cl, Br, I) to soluble nanowires, by introducing oppositely charged synthetic lipids as lipophilic counterions.⁶ This lipid-covering methodology has been successfully applied to a variety of 1D metal complexes.⁷ An alternative approach to convert 1D coordination complexes soluble in organic media is to covalently attach lipophilic alkyl chains to the bridging ligands, as demonstrated for transition metal 1,2,4-triazole complexes.⁸ These lipophilic coordination nanowires show unique features such as formation of 1D electronic structures in response to self-assembly,^{6,7a} supramolecular band gap engineering,^{6f,g} solvatochromism,^{6h,j} heat-set gelation of organic solvents,^{8a} photoresponsive properties,^{8b} solvophobically controlled spin conversion,^{7a} and formation of

Received: October 1, 2011

Published: December 13, 2011



stereohoneycomb nanoarchitectures under far-from-equilibrium conditions.^{6g} Thus, the conversion of solid-state pseudo-1D metal complexes to lipophilic supramolecular polymers opened a new dimension in coordination nanochemistry.

To control macroscopic orientation of nanowires, the use of shear stress⁹ and electrostatic absorption onto oppositely charged surface patterns¹⁰ have been demonstrated. These approaches, however, are less satisfactory in precisely controlling their anisotropic alignments. In addition, the electrostatic adsorption technique requires preparation of charged surface patterns, and consequently, it is only applicable to charged nanowires. Although nanofabrication techniques like dip-pen lithography possess exquisite atomic manipulation abilities,¹¹ most scanning probes are slow and have limitations in high-throughput fabrication. On the other hand, electric fields have been used to align anisotropic nanomaterials such as carbon nanotubes (CNTs),^{12–14} inorganic nanowires,^{15–18} biopolymers,^{19,20} and organic supramolecular fibers dispersed in solution.^{21–23} Dielectrophoretic (DEP) force is generated under nonuniform ac electric fields, which allowed assembly of dielectric particles.^{12–16,18,19,22} Thus, electric field offers a simple and practical way to align nanowires in between opposing electrodes. However in spite of these advantages, to the best of our knowledge, electric field has not been applied to control macroscopic orientation of metal complexes in solution or in liquid crystalline mesophases.²⁴

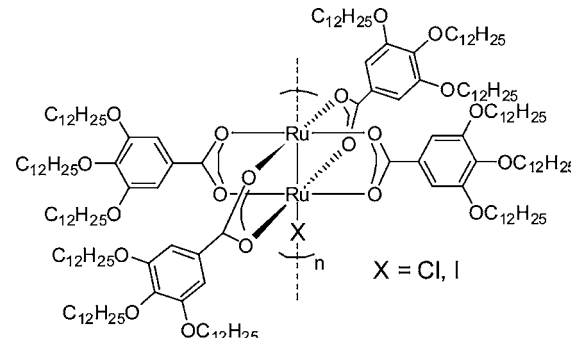
In this study, we report self-assembly and electric-field assisted unidirectional orientation of halogen-bridged, mixed-valence diruthenium complexes $\text{Ru}_2(\mu\text{-O}_2\text{CR})_4\text{X}$ ($\text{RCOO} = 3,4,5\text{-tridodecyloxybenzoate}$, $\text{X} = \text{Cl}, \text{I}$) in organic media. The diruthenium complex $\text{Ru}_2(\mu\text{-O}_2\text{CR})_4\text{X}$ belongs to a family of MMX-chain complexes which show a rich variety of electronic structures^{1,2} and magnetic characteristics.^{3,4} Because of the strong electronic interaction in diruthenium units, they generally reveal averaged valence electronic structure $(-\text{Ru}^{2+}-\text{Ru}^{2.5+}-\text{X}-)_n$ with a quadruplet ground state ($S = 3/2$), where three unpaired electrons adopt a high spin $(\delta^*)^1(\pi^*)^2$ electron configuration.²⁵ Although these unique structural and electronic features are promising for developing nanowire devices, they are parts of bulk crystals and dissolution of RuRuX complexes in polar solvents resulted in the dissociation of coordination chains into $[\text{Ru}-\text{Ru}(\text{solvent})_2]^+$ and X^- species.²⁶ Meanwhile, Zamora et al. recently reported atomic force microscopy (AFM) observation of $\text{Ru}_2(\mu\text{-O}_2\text{CC}_2\text{H}_5)_4\text{X}$ complexes which are spread on solid substrates by casting aqueous micelle solutions ($\text{X} = \text{Br}$)^{27a} or ultrasonicated ethanol solutions ($\text{X} = \text{I}$).^{27b} The propionate equatorial ligands employed in these studies are discernibly short in order to gain sufficient van der Waals interactions and solubility in organic media, which are required to disperse them as coordination polymers. Consequently, these systems suffer from the undesirable use of surfactants and highly coordinating solvent such as ethanol. Moreover, coordination polymers cast on solid supports from these solutions show no orientational order. Although Rusjan et al. reported mesophase behavior of chloro-bridged diruthenium(II,III) 3,4,5-tetradecyloxybenzoates in *n*-dodecane,²⁸ control on their electronic structures, self-assembly and macroscopic orientation have not been achieved. Here we show axial halogen ligands $\text{X} (= \text{Cl}, \text{I})$ in $\text{Ru}_2(\mu\text{-O}_2\text{CR})_4\text{X}$ show crucial influences on the self-assembly of diruthenium complexes, electronic structures of resultant coordination chains and on their dielectrophoretic alignment

characteristics in organic media. These observations provide valuable guidelines in designing electric-field-responsive coordination nanowires.

RESULTS AND DISCUSSION

Self-Assembly in Solution. Halogen bridged, lipophilic diruthenium complexes **1**($\text{X} = \text{Cl}$), **2**($\text{X} = \text{I}$) having four 3,4,5-tridodecyloxybenzoate ligands per Ru–Ru–X unit were newly synthesized (Chart 1). These complexes are soluble in

Chart 1. Unit Molecular Structure of Halogen-Bridged Coordination Polymers **1**($\text{X} = \text{Cl}$) and **2**($\text{X} = \text{I}$)



nonpolar solvents such as *n*-decane, cyclohexane and toluene. The two axial halogen ligands ($\text{X} = \text{Cl}, \text{I}$) were introduced with an aim to control their hierarchical self-assembly into coordination wires and further to lyotropic liquid crystals in organic media, their electronic structures and dielectrophoretic properties. When **1**($\text{X} = \text{Cl}$) and **2**($\text{X} = \text{I}$) were dispersed in *n*-decane at concentrations above 100 mM, birefringent liquid crystals were obtained. In small-angle X-ray (SAXS) diffraction data obtained for **1**($\text{X} = \text{Cl}$) in *n*-decane (Figure S1(a) in the Supporting Information), a series of sharp scattering peaks are observed at $2\theta = 0.30, 0.51, 0.59$, and 0.78° , with a *d*-spacing ratio of $1:3^{1/2}:4^{1/2}:7^{1/2}$. The small-angle diffractions are related to the intercolumnar distances, and the observed higher order diffraction peaks are indexed as (100), (110), (200), and (210) diffractions. It clearly demonstrates the presence of highly ordered hexagonal columnar arrangement (Col_h) with long-ranged structural order. The distance between centers of each cylinder is determined as 3.46 nm, which is smaller than the width of molecular wire **1** (width ~4.75 nm, Supporting Information, Figure S1(c, d)). It suggests interdigititation of side alkylchains between hexagonally aligned coordination polymers, which enhances intercolumnar interactions.²⁸ The interdigititation between peripheral alkyl chains require the presence of void spaces around Ru–Ru–Cl coordination chains, which would be facilitated when main chains assume zigzag conformation.²⁹ On the other hand, **2**($\text{X} = \text{I}$) dispersed in *n*-decane (100 mM) exhibited a distinct broad XRD peak which correspond to an intercolumnar distance of 5.2 nm (Supporting Information, Figure S1(b)). This distance is larger than the width of molecular wire of **2**. It apparently indicates that peripheral alkyl chains of coordination polymer **2**($\text{X} = \text{I}$) are not interdigitated but are swelled by absorption of *n*-decane molecules. It resulted in the decreased lateral positional order as indicated by the broadness of the XRD reflection peak, which is characteristic of columnar nematic phase (Col_n). The LC phases observed for **1**($\text{X} = \text{Cl}$) and **2**($\text{X} = \text{I}$) in *n*-decane were obtained above the concentration of ~100 mM, whereas

isotropic dispersions were obtained below this concentration as indicated by disappearance of the birefringence and SAXS peaks.

Figure 1a shows the visible spectra of **1**(X = Cl) observed for *n*-decane solutions at different concentrations of 0.01 mM, 0.1 mM, and 1 mM.

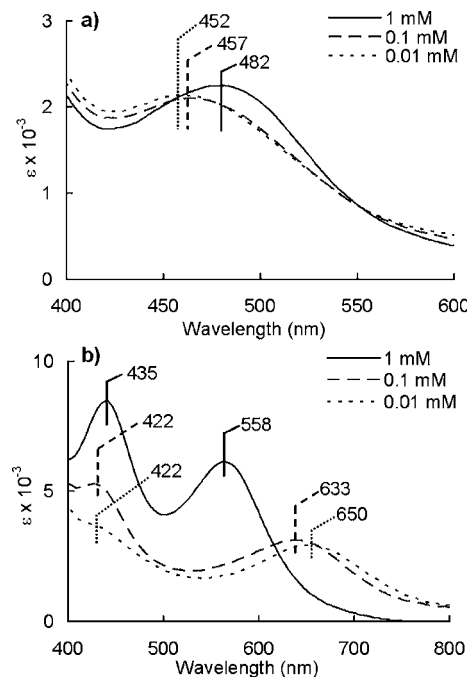


Figure 1. Visible spectra of (a) **1**(X = Cl) and (b) **2**(X = I) at concentrations of 0.01 mM, 0.1 mM, and 1 mM in *n*-decane. Temperature: 20 °C.

mM and 1 mM (temperature, 25 °C). An intense absorption peak is observed around at 450–500 nm, which is ascribed to the $\pi(\text{RuO}_\text{2}, \text{Ru}_\text{2}) \rightarrow \pi^*(\text{Ru}_\text{2})$ transition polarized along the coordination chain.²⁵ At 0.01 mM, the $\pi(\text{RuO}_\text{2}, \text{Ru}_\text{2}) \rightarrow \pi^*(\text{Ru}_\text{2})$ absorption showed a maximum at 452 nm. This absorption maximum is identical with that observed for toluene solution (concentration, 0.5 mM to 3 mM), in which **1**(X = Cl) is dispersed as a unit paddlewheel complex as confirmed by vapor pressure osmometry. The peak around at 452 nm is also reported for a monomeric long-chained $[\text{Ru}_\text{2}(\text{O}_2\text{CR})_4\text{Cl}]$ complexes (i.e., R = $-\text{C}_{11}\text{H}_{23}$) in CH_2Cl_2 which is coordinated with one chloride ion in the axial position.³⁰ Therefore, the observed $\pi(\text{RuO}_\text{2}, \text{Ru}_\text{2}) \rightarrow \pi^*(\text{Ru}_\text{2})$ absorption peak at 452 nm in 0.01 mM *n*-decane is reasonably assignable to monomeric unit diruthenium complex of **1**(X = Cl). On the other hand, upon increasing the concentration to 1 mM, the peak shifted to 482 nm. This peak is identical to those observed for cast films and matches with the reported absorption maxima for pseudo one-dimensional complexes in the solid state.²⁶ These observations clearly indicate that the observed red shift in $\pi(\text{RuO}_\text{2}, \text{Ru}_\text{2}) \rightarrow \pi^*(\text{Ru}_\text{2})$ absorption reflects polymerization of unit complex **1**(X = Cl) in *n*-decane at higher concentrations.

In Figure 1b, absorption spectra of **2**(X = I) in *n*-decane at varied concentrations are shown. At low concentration of 0.01 mM, the $\pi(\text{RuO}_\text{2}, \text{Ru}_\text{2}) \rightarrow \pi^*(\text{Ru}_\text{2})$ absorption band is observed at 650 nm. Upon increasing the concentration to 0.1 mM, the peak shifted to 633 nm with enhancement in peak intensity at 422 nm. The 422 nm-peak is attributed to $\pi(\text{axial ligand}) \rightarrow \pi^*(\text{Ru}_\text{2})$ absorption²⁶ and the observed peak wavelengths are

similar to those reported for a molecularly dispersed unit paddlewheel complexes with one axial position occupied by an iodide ion. Interestingly, when the concentration is further raised to 1 mM, the absorption peaks of $\pi(\text{axial ligand}) \rightarrow \pi^*(\text{Ru}_\text{2})$ and $\pi(\text{RuO}_\text{2}, \text{Ru}_\text{2}) \rightarrow \pi^*(\text{Ru}_\text{2})$ bands shifted to 435 and 558 nm, respectively with considerable increase in the absorption intensity. Although spectral data for iodo-bridged polymeric complex $\text{Ru}_\text{2}(\mu\text{-O}_2\text{CR})_4\text{I}$ have not been reported to date, we assign the observed salient spectral changes to polymerization of **2**(X = I) in *n*-decane, based on the measurement of temperature-dependent visible spectra as described below.

Figure 2 shows temperature dependence of visible absorption spectra observed for **1**(X = Cl) (a) and **2**(X = I) (b) in *n*-

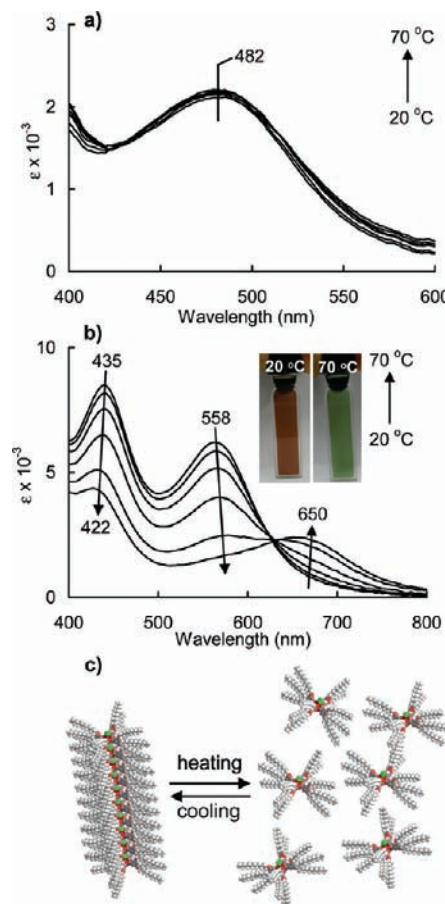


Figure 2. Temperature dependence of visible spectra for (a) **1**(X = Cl) and (b) **2**(X = I). concentration, 1 mM in *n*-decane (cell width, 0.1 mm). Spectra are recorded from 20 °C at every 10 °C. (c) Schematic illustration of thermally controlled self-assembly of columnar nematic **2**(X = I) in decane.

decane (1 mM). **1**(X = Cl) showed almost no spectral changes in the temperature range of 20–70 °C (Figure 2a). It indicates that the polymeric ($\text{Ru}-\text{Ru}-\text{Cl}$)_n structure is thermally intact even at elevated temperatures. In contrast, **2**(X = I) in decane showed salient thermochromism. The dark brown color observed at room temperature turned green upon heating (pictures in Figure 2b). The color change observed upon heating is ascribed to the decrease in absorption intensities at 435 and 558 nm, which shifted to 422 and 650 nm respectively with an isosbestic point appearing around at 625 nm (Figure 2b). The 422 nm and 650 nm peaks observed at 70 °C are

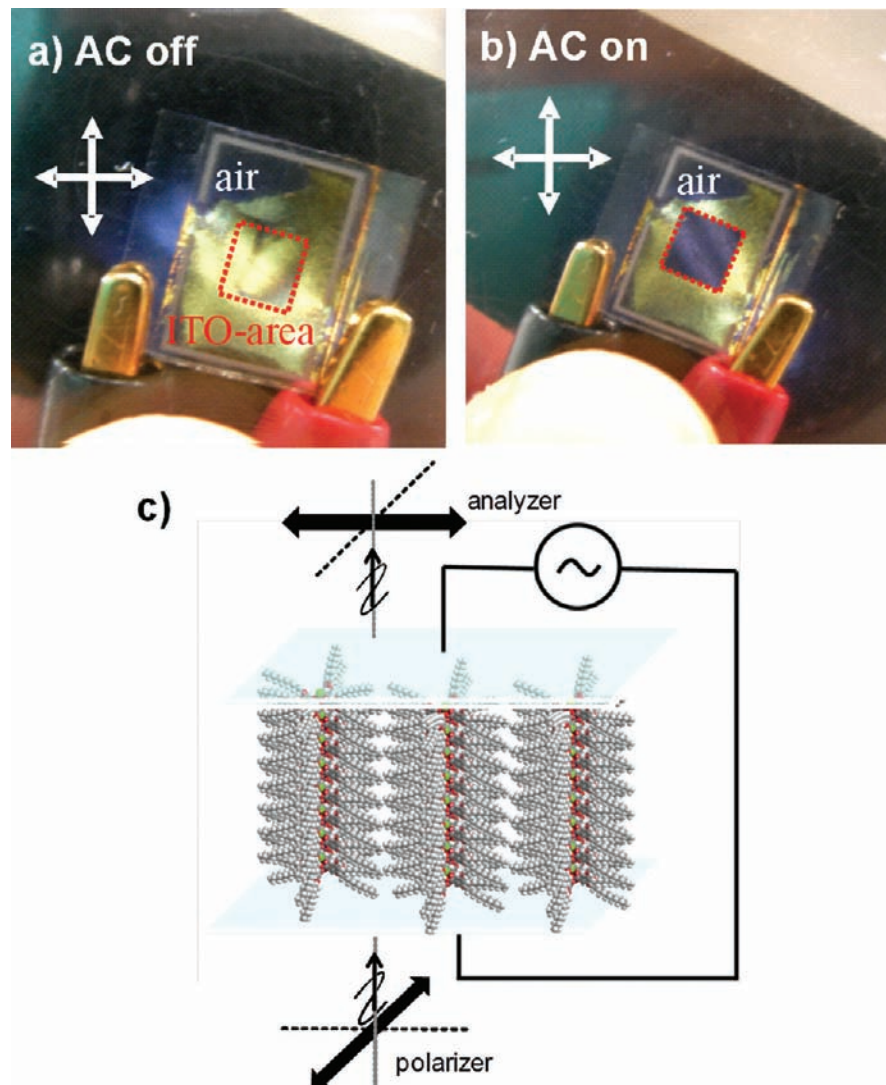


Figure 3. Pictures of decane solution of **1**(X = Cl) sandwiched between ITO cell under crossed polarizers. (a) Picture before applying ac electric field. An area surrounded by a box in red broken line indicates the ITO-electrode coated area. A set of orthogonally oriented polarizers were placed above and under the ITO cell and the double-arrows indicate the configuration of the polarizers. The darker portion in upper left of the cell is ascribed to air bubble. (b) Picture after applying ac electric field ($0.8 \text{ V } \mu\text{m}^{-1}$, 100 Hz) between ITO electrodes. ITO-electrode area surrounded by a box in red broken line does not show light transmission under crossed polarizers. (c) Schematic illustration of coordination nanowires homeotropically aligned between ITO electrodes under the ac electric field. The sample **1**(X = Cl, 100 mM in decane) was filled between ITO electrodes with a thickness of 20 μm .

identical to those observed for dilute 0.01 mM solution (Figure 1b), indicating that the polymeric structure of **2**(X = I) dissociates into unit paddlewheel complexes at elevated temperatures. On the other hand, cooling of the solution to room temperature reversibly afforded the original absorption spectra with peaks located at 435 and 558 nm (Supporting Information, Figure S2). These observations clearly demonstrate that iodo-bridged coordination polymers in columnar nematic mesophase show thermally reversible self-assembly: they dissociate into discrete paddlewheel complexes by heating and reassemble upon cooling (Figure 2c).

Thus, axial halide ligands X (Cl or I) in $(\text{Ru}-\text{Ru}-\text{X})_n$ polymers play crucial roles in determining 1D electronic structures, integrity of coordination chains, intercolumn interactions and accordingly their thermal self-assembling characteristics in organic media. It is apparent that iodine ions show weaker coordination ability to bridge paddlewheel $\text{Ru}_2(\mu-\text{O}_2\text{CC}_6\text{H}_5)_4$ units compared to chloride ions.³¹ This is

consistent with a number of one-dimensional structures reported for chloro-bridged $[\text{Ru}_2(\mu-\text{O}_2\text{CR})_4\text{Cl}]_n$ complexes in the solid state,^{2–5} whereas reports on polymeric coordination structures of iodo-bridged complexes have been surprisingly limited to tetrakisbenzoate $[\text{Ru}_2(\mu-\text{O}_2\text{CC}_6\text{H}_5)_4\text{I}]$ and tetrakis-propionate $[\text{Ru}_2(\mu-\text{O}_2\text{C}_2\text{H}_5)_4\text{I}]$ complexes.^{26,27b}

Dielectrophoretic Alignment. To regulate macroscopic orientation of coordination polymers **1**(X = Cl) and **2** (X = I) in *n*-decane, alternating electric field was applied at different voltages and frequencies (Hz). The indium tin oxide (ITO) electrode used to apply ac voltage is schematically shown in Figure S3 (Supporting Information). **1**(X = Cl) and **2**(X = I) dispersed in *n*-decane (100 mM) were filled between ITO-coated glass slides (thickness, 20 μm , ITO electrode-coated area shown in red broken line, 5 mm \times 5 mm) which were placed between a set of crossed polarizers. Figure 3 shows appearance of *n*-decane solution of **1**(X = Cl) confined in the ITO-coated cell. The *n*-decane dispersion showed significant

light transmission between crossed polarizers due to optical birefringence revealed by the hexagonal columnar phase (Figure 3a). On the other hand, upon applying ac electric field to the electrodes ($0.8 \text{ V } \mu\text{m}^{-1}$, 100 Hz), birefringence of the sample under ITO electrodes immediately disappeared and turned dark (Figure 3b). It indicates that coordination nanowires are homeotropically aligned in the direction of the electric field, i.e., oriented perpendicularly to the ITO electrodes as schematically illustrated in Figure 3c.

Figure 4 compares time dependence of transmitted light intensity for **1**(X = Cl) and **2**(X = I) after applying ac electric

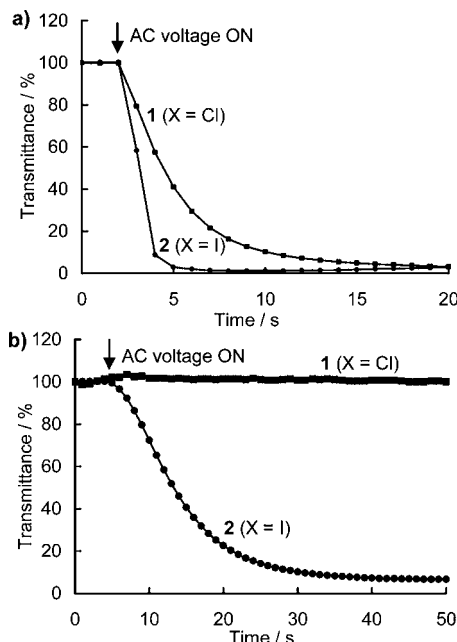


Figure 4. Time dependence of the light transmittance after applying ac electric field. Key: (a) at $0.8 \text{ V } \mu\text{m}^{-1}$, 100 Hz and (b) at $0.25 \text{ V } \mu\text{m}^{-1}$, 100 Hz. $[1(\text{X} = \text{Cl})] = [2(\text{X} = \text{I})] = 100 \text{ mM}$ in *n*-decane. Light transmittance was measured by using Otsuka electronics MCPD-1000 with optical set up shown in Figure 3, with liquid crystal cell placed in between the two crossed polarizers. The vertical scale is normalized to the light intensity before applying electric field. The decrease in transmittance is ascribed to homeotropic alignment of coordination nanowires induced by the electric field.

fields of (a) $0.8 \text{ V } \mu\text{m}^{-1}$ and (b) $0.25 \text{ V } \mu\text{m}^{-1}$, respectively (concentration, 100 mM). Application of the ac electric field of $0.8 \text{ V } \mu\text{m}^{-1}$ (100 Hz) elicits a response from **1**(X = Cl), and time required for **1**(X = Cl) to adopt homeotropic alignment was within ~ 15 s (Figure 4a). On the other hand, **2**(X = I) showed much faster response and coordination nanowires were oriented homeotropically within ~ 2 s (Figure 4a). Even under a weaker ac electric field of $0.25 \text{ V } \mu\text{m}^{-1}$, **2**(X = I) showed a drop in the light transmission within ~ 30 s (Figure 4b). This is in remarkable contrast to **1**(X = Cl) which revealed no response under this weak applied voltage (Figure 4b). These observations clearly indicate that **2**(X = I) in columnar nematic phase show higher responsiveness to the applied ac electric field. Figure S4 and S5 (Supporting Information) show time dependences of the light transmission observed for **2**(X = I) at varied applied voltages (0.1 – $0.8 \text{ V } \mu\text{m}^{-1}$, at 100 Hz) and frequencies (0 – 5000 Hz, at $0.25 \text{ V } \mu\text{m}^{-1}$). Appreciable drop in transmittance occurred above the applied voltage of $0.1 \text{ V } \mu\text{m}^{-1}$ and it became faster under larger electric field (Figure S4 in

Supporting Information). On the other hand, the drop in the transmittance occurs most effectively in the frequency range of 10–100 Hz and the ac-electric field induced homeotropic alignment is suppressed at frequencies both below 2 Hz or above 1000 Hz. This frequency dependence is reasonable since orientational changes of coordination nanowires require dielectric torque imposed by the electric field, which is weaker at low-frequencies. On the other hand, the coordination polymers cannot follow the high-frequency electric field above ~ 1000 Hz.

Remarkable difference was also observed in recovery profiles of the light transmission after turning off the electric field (Figure S6, Supporting Information). In the case of **1**(X = Cl), intensity of the transmitted light after turning off the electric field showed slow increase within ~ 15 min and it leveled off at ca. 48% of the initial light intensity. The decrease in transmittance occurred in every recovery cycles and after three cycles, it was reduced to ca. 5% of the initial intensity. Consistent with the observed decrease in transmittance upon repetitive application of external electric field, crossed polarizing optical microscopy image under ITO-electrode showed increase in the fraction of darker area (right side in Figure S6b, Supporting Information). It indicates that homeotropically aligned coordination nanowires are accumulated without relaxing into random orientation, after switching off the applied electric field. It reflects larger interchain interactions between hexagonally oriented coordination polymers of **1**(X = Cl). In contrast, **2**(X = I) in *n*-decane showed reversible changes in the intensity of transmitted light even at the weak electric field of $0.25 \text{ V } \mu\text{m}^{-1}$ (Figure S6c, Supporting Information). It is noteworthy that columnar nematic phase of **2**(X = I) show higher responsiveness to the applied ac field, compared to ordered columnar hexagonal phase formed from **1**(X = Cl). These observations clearly indicate that homeotropic orientation of coordination nanowires depends on interactions between coordination nanowires and consequent viscoelastic character of lyotropic liquid crystals. The weaker bridging ability of axial iodide ions would lead to enhanced flexibility of the $(-\text{Ru}-\text{Ru}-\text{I}-)_n$ chains, which is seemingly unfavorable for peripheral alkyl chains to interdigitate between nanowires. As a result, **2**(X = I) formed the swollen columnar nematic (Col_n) phase with enhanced responsiveness to the applied electric field.

To further control macroscopic orientation of coordination nanowires in two dimension, ac electric field was applied to *n*-decane solution of **1**(X = Cl) placed in between a set of parallel-oriented copper electrodes separated with a gap of $100 \mu\text{m}$ (Figure 5a). To evaluate electric field-induced lateral anisotropy, transmittance of polarized light was observed by attaching a polarizer under the *n*-decane solution. The solution show brown color due to the $\pi(\text{RuO}_x, \text{Ru}_2) \rightarrow \pi^*(\text{Ru}_2)$ absorption, is most darkly observed when the plane of polarized light is fixed parallel to the electric field (Figure 5c). On the other hand, the highest transmittance was obtained when polarizers are oriented perpendicular to the electric field (Figure 5b). As the $\pi(\text{RuO}_x, \text{Ru}_2) \rightarrow \pi^*(\text{Ru}_2)$ transition is oriented along the linear coordination chain, these observations clearly indicate that main chain of coordination polymer **1**(X = Cl) are oriented in the direction of electric field, that is, perpendicular to the opposing electrode edges.

Interestingly, the dielectrophoretic alignment of coordination polymer **1** was observed also for dilute isotropic solution (concentration, 20 mM, Supporting Information, Figure S7). At

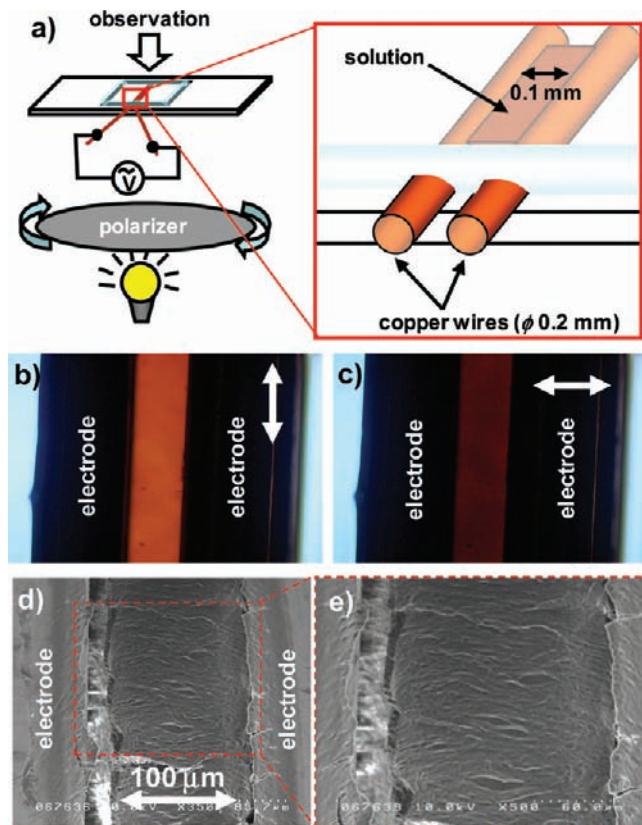


Figure 5. (a) Schematic illustration of the experimental cell for investigating optical anisotropy of coordination nanowires under applied ac electric field (50 V, 100 Hz). Two copper wire electrodes (diameter, 0.2 mm) are placed parallel in between glass plates with a gap of 100 μm . *n*-decane solutions of **1**(X = Cl, concentration, 100 mM or 20 mM) were filled between the electrodes and the cell was sealed by using adhesives to prevent evaporation of the solvent. (b, c) Polarizing microscope images of decane solution of **1**(X = Cl) (concentration, 100 mM): (b) optical axis of polarizer set perpendicular to the direction of electric field; (c) optical axis of polarizer fixed parallel to the applied electric field. (d, e) Scanning electron micrographs of **1**(X = Cl) immobilized between opposing electrodes. The specimen was prepared by freeze-drying cyclohexane solution of **1**(X = Cl, 100 mM) under the applied ac electric field.

this concentration, coordination polymer **1** (X = Cl) is molecularly dispersed without forming liquid crystals. At zero voltage, the *n*-decane solution of **1** did not transmit light. It indicates that the coordination polymers are dissolved without anisotropic alignment, as can be seen from the dark image observed under crossed polarizers (Figure S7a, Supporting Information). In contrast, the highest transmittance was immediately obtained after applying the ac electric field (100 V, 20 Hz, Figure S7b). The change in optical transmission was quickly turned on-and-off in response to the applied electric field, which was much faster than those observed for the 100 mM lyotropic liquid crystalline dispersion. These observations confirm that polarization forces produced by the alternating electric field induce motion and reorientation of molecularly dispersed coordination nanowires.

To observe anisotropically aligned coordination polymers under the applied ac electric field, they were immobilized by freeze-drying technique and were viewed by scanning electron microscopy (SEM). Cyclohexane was selected as a solvent because it is facilely sublimated under reduced pressure. A

lyotropic cyclohexane solution of **1**(X = Cl, 100 mM) was injected between opposing copper electrodes as described above. After applying ac electric field (50 V, 100 Hz, for 1 min) in a Petri dish saturated with cyclohexane vapor, the sample was rapidly cooled in liquid nitrogen and freeze-dried at -15°C under vacuum. Figure 5(d,e) shows SEM pictures of the specimen. In spite of the possible disarray caused by the freeze-drying procedure, macroscopically oriented fibrous structures were observed between electrodes. These fibrous structures appears to have a continuous structure over a length of $\sim 100 \mu\text{m}$, in agreement with the macroscopic anisotropy observed in Figure 5(b,c). With the present parallel electrode geometry in nonpolar organic media, the electric field and the field gradient is expected to be larger near the electrodes. That is, the field strength would decrease for larger distances from the electrodes. Therefore, the long-ranged macroscopic orientation of nanofibers observed in between electrodes (Figure 5d,e) indicates the presence of end-to-end interactions between hexagonally aligned columnar structures. The combination of lipophilic coordination chains and electrophoretic force thus provide a useful means to hierarchically self-assemble metal complexes over scales ranging from a molecule to micrometer-sized anisotropic architectures.

CONCLUSION

In summary, mixed-valence diruthenium paddlewheel complexes self-assemble in organic media to give halogen-bridged supramolecular polymers, which are hierarchically developed into columnar hexagonal structure (for **1**(X = Cl)) or nematic columnar phase (for **2**(X = I)). The halogen axial ligands exert decisive roles to determine 1D electronic structures, integrity of polymeric coordination chains, interchain interactions and hierarchical self-assembly. They also affect responsiveness to the applied electric field. The self-assembly of coordination polymers and application of ac electric field provide a versatile means to control their macroscopic orientation over a large area. The integration of bottom-up and top-down approaches as shown in this study would be widely applicable to push back the frontiers of coordination nanomaterials chemistry.

EXPERIMENTAL SECTION

Materials. *Synthesis of Tetrakis(μ -3,4,5-tridecyloxybenzoyloxy)diruthenium Chloride **1**(X = Cl).* Chlorotetrakis(acetate) diruthenium(II,III) Ru₂(μ -O₂CCH₃)₄Cl²⁹ and 3,4,5-tridecyloxybenzoic acid³² was prepared according to the previous reports. To a solution of 3,4,5-tridecyloxybenzoic acid (639 mg, 1.26 mmol) in dichloromethane (15 mL) was added chlorotetrakis(acetate) diruthenium (100 mg, 0.21 mmol), ethanol (5 mL), and water (20 mL) under an nitrogen atmosphere. After the mixture was vigorously stirred for 8 h at ambient temperature, the organic phase was separated and dried over anhydrous sodium sulfate. The solvent was removed under reduced pressure and residual solid was purified by silica gel chromatography eluted with dichloromethane. **1** was obtained in 81% yield (384 mg, 0.17 mmol) as brown waxy solid. IR (ATR, cm^{-1}) 2920 (ν_{CH}), 2852 (ν_{CH}), 1586 ($\nu_{\text{C=C}}$), 1452, 1410, 1371, 1229, 1113, 769, 720. MALDI-TOF-MS (dithranol, positive), *m/z*: calcd for C₁₂₄H₂₁₂O₂₀Ru₂, [(M - Cl)⁺], 2225; found, 2222. Anal. Calcd for C₁₂₄H₂₁₂ClO₂₀Ru₂: C, 65.88; H, 9.45. Found: C, 65.85, H, 9.4.

Synthesis of Tetrakis(μ -acetoxyl)diruthenium Iodide. To a suspension of Ru₂(μ -O₂CCH₃)₄Cl (400 mg, 0.84 mmol) in dry THF (50 mL) was added silver tetrafluoroborate (197 mg, 1.01 mmol) under an argon atmosphere. After the mixture was stirred for 12 h at room temperature, silver chloride precipitated was filtered off and aqueous potassium iodide (3.50 g, 21.1 mmol/20 mL) was added to

this brown solution. The precipitates formed immediately were collected by filtration and washed with saturated aqueous potassium iodide (10 mL), water (10 mL), and then methanol (5 mL) to give $\text{Ru}_2(\mu\text{-O}_2\text{CCH}_3)_4\text{I}$ in 80% yield (382 mg, 0.68 mmol) as dark gray solid. IR (ATR, cm^{-1}) 1431, 1394, 1344, 1049, 688. MALDI-TOF-MS (dithranol, positive), m/z : calcd for $\text{C}_8\text{H}_{12}\text{O}_8\text{Ru}_2$, [(M - I)⁺], 440; found, 440. Anal. Calcd for $\text{C}_8\text{H}_{12}\text{IO}_8\text{Ru}_2$: C, 17.00; H, 2.14. Found: C, 17.02; H, 2.10.

Synthesis of Tetrakis(3,4,5-tridodecyloxybenzoyloxy)diruthenium Iodide 2(X = I). $\text{Ru}_2(\mu\text{-O}_2\text{CCH}_3)_4\text{I}$ (100.0 mg, 0.18 mmol) and 3,4,5-tridodecyloxybenzoic acid (716.6 mg, 1.06 mmol) were added dichloromethane (20 mL), ethanol (5 mL), and water (50 mL) under an nitrogen atmosphere. The mixture was stirred at room temperature for 12 h. At the end of reaction, the solid of $\text{Ru}_2(\mu\text{-O}_2\text{CCH}_3)_4\text{I}$ completely disappeared and the organic phase turned to dark purple. The organic phase was dried over anhydrous sodium sulfate and evaporated in vacuo to dryness. The residual brown solid was purified by silica gel chromatography eluted with dichloromethane to give 2(X = I) in 49% yield (266.8 mg, 0.088 mmol) as dark brown solid. IR (ATR, cm^{-1}) 2920 (ν_{CH}), 2852 (ν_{CH}), 1586 ($\nu_{\text{C=C}}$), 1451, 1410, 1371, 1229, 1113, 769, 720. MALDI-TOF-MS (dithranol, positive), m/z : calcd for $\text{C}_{172}\text{H}_{308}\text{O}_{20}\text{Ru}_2$, [(M - I)⁺], 2898; found, 2897. Anal. Calcd for $\text{C}_{172}\text{H}_{308}\text{IO}_{20}\text{Ru}_2$: C, 68.29; H, 10.26. Found: C, 68.56, H, 10.30.

Measurements. Matrix-assisted laser desorption ionization time-of-flight mass spectrometry (MALDI-TOF-MS) was performed on a Bruker Autoflex-III. Elemental analysis was conducted at the Elemental Analysis Center, Kyushu University. For small-angle X-ray scattering (SAXS) of 1D complexes dispersed in *n*-decane, the solutions were loaded into 0.7 mm diameter capillaries (Markrohrchen aus Glas Nr. 14, length, 80 mm, thickness, 0.01 mm, Hilgenberg GmbH). The sample was then exposed to synchrotron X-ray radiation of wavelength 0.9 Å at BL40B2 in the SPring-8 (operation energy of 8 GeV and stored current of 100 mA, $\lambda = 1.0$ Å). Vapor pressure osmometry was performed on GONOTEC OSMOMAT 070. Polarized optical microscopy and scanning electron microscopy (SEM) and was conducted on a Nikon ECLIPSE 80i and Hitachi S-5000, respectively. The ac electric field was generated by WF1944B and amplified by HSA4051 (NF Corporation). Electric field-assisted alignment measurements were performed by using commercially available electro-optical cell covered with indium tin oxide (ITO) (INSTEC LC2-20.0, cell thickness, 20 μm) or a handmade cell integrated in the optical microscope. In the handmade cell, two copper wire electrodes (ϕ 0.2 mm) were placed parallel on a glass substrate with a gap of 100 μm , and a cover glass was placed on these electrodes. After injection of lyotropic liquid crystals of 1(X = Cl) or 2(X = I) in *n*-decane (concentration, 100 mM) between the electrodes, the cell was sealed by using adhesives to prevent evaporation of the solvent. Ac voltage was applied to the samples at frequencies of 0–10 kHz, and the specimens were observed *in situ* under the polarizing microscope. The coordination polymers macroscopically aligned under the electric field was immobilized by applying freeze-drying technique (at -15 °C for 4 h).

ASSOCIATED CONTENT

Supporting Information

Experimental details, XRD and vis spectra, crossed polarized pictures of 2(X = I) in *n*-decane under ac electric field, voltage and frequency dependences of light transmittance, temporal transmission light intensity responses and polarizing optical micrographs upon switching on–off the applied electric field. This material is available free of charge via the Internet at <http://pubs.acs.org>.

AUTHOR INFORMATION

Corresponding Author

n-kimi@mail.cstm.kyushu-u.ac.jp

Present Address

[#]International Institute for Carbon-Neutral Energy Research, Kyushu University, 744 Moto-oka, Nishi-ku, Fukuoka 819-0395, Japan.

ACKNOWLEDGMENTS

This work was financially supported by JST CREST.

REFERENCES

- (1) *Nanochemistry*; Ozin, G. A.; Arsenault, A. C. RSC Publishing: Cambridge, U.K., 2005.
- (2) Matsuzaki, H.; Matsuoka, T.; Kishida, H.; Takizawa, T.; Miyasaka, H.; Sugura, K.; Yamashita, M.; Okamoto, H. *Phys. Rev. Lett.* **2003**, 90, 046401.
- (3) Kitagawa, H.; Onodera, N.; Sonoyama, T.; Yamamoto, M.; Fukawa, T.; Mitani, T.; Seto, M.; Maeda, Y. *J. Am. Chem. Soc.* **1999**, 121, 10068.
- (4) Mitsumi, M.; Kitamura, K.; Morinaga, A.; Ozawa, Y.; Kobayashi, M.; Toriumi, K.; Iso, Y.; Kitagawa, H.; Mitani, T. *Angew. Chem., Int. Ed.* **2002**, 41, 2767.
- (5) Cukiernik, F. D.; Luneau, D.; Marchon, J. -C.; Maldivi, P. *Inorg. Chem.* **1998**, 37, 3698.
- (6) (a) Kimizuka, N. *Adv. Mater.* **2000**, 12, 1461. (b) Kimizuka, N. In *Supramolecular Polymers*, 2nd ed.; Ciferri, A., Ed.; Taylor & Francis/CRC Press: Boca Raton, FL, 2005. (c) Kimizuka, N. *Adv. Polym. Sci.* **2008**, 219, 1. (d) Kimizuka, N.; Oda, N.; Kunitake, T. *Chem. Lett.* **1998**, 8, 695. (e) Kimizuka, N.; Lee, S. H.; Kunitake, T. *Angew. Chem., Int. Ed.* **2000**, 39, 389. (f) Kimizuka, N.; Oda, N.; Kunitake, T. *Inorg. Chem.* **2000**, 39, 2684. (g) Lee, C. -S.; Kimizuka, N. *Proc. Natl. Acad. Sci. U.S.A.* **2002**, 99, 4922. (h) Lee, C.-S.; Kimizuka, N. *Chem. Lett.* **2002**, 12, 1252. (i) Yasui, K.; Kimizuka, N. *Chem. Lett.* **2005**, 34, 248. (j) Kuroiwa, K.; Oda, N.; Kimizuka, N. *Sci. Tech. Adv. Mater.* **2006**, 7, 629.
- (7) (a) Matsukizono, H.; Kuroiwa, K.; Kimizuka, N. *J. Am. Chem. Soc.* **2008**, 130, 5622. (b) Meister, A.; Frster, G.; Thnemann, A. F.; Kurth, D. G. *ChemPhysChem* **2003**, 4, 1095. (c) Bodenthin, Y.; Pietsch, U.; Möhwald, H.; Kurth, D. G. *J. Am. Chem. Soc.* **2005**, 127, 3110. (e) Bodenthin, Y.; Schwarz, G.; Tomkowicz, Z.; Geue, T.; Haase, W.; Pietsch, U.; Kurth, D. G. *J. Am. Chem. Soc.* **2009**, 131, 2934. (d) Schwarz, G.; Bodenthin, Y.; Tomkowicz, Z.; Haase, W.; Geue, T.; Kohlbrecher, J.; Pietsch, U.; Kurth, D. G. *J. Am. Chem. Soc.* **2011**, 133, 547.
- (8) (a) Kuroiwa, K.; Shibata, T.; Takada, A.; Nemoto, N.; Kimizuka, N. *J. Am. Chem. Soc.* **2004**, 126, 2016. (b) Kume, S.; Kuroiwa, K.; Kimizuka, N. *Chem. Commun.* **2006**, 2442. (c) Matsukizono, H.; Kuroiwa, K.; Kimizuka, N. *Chem. Lett.* **2008**, 37, 446. (d) Kuroiwa, K.; Kimizuka, N. *Chem. Commun.* **2010**, 46, 1229. (e) Kuroiwa, K.; Kimizuka, N. *Chem. Lett.* **2010**, 39, 790.
- (9) Liu, L. M.; Singh, M.; John, V. T.; McPherson, G. L.; He, J. B.; Agarwal, V.; Bose, A. *J. Am. Chem. Soc.* **2004**, 126, 2276.
- (10) Myung, S.; Lee, M.; Kim, G. T.; Ha, J. S.; Hong, S. *Adv. Mater.* **2005**, 17, 2361.
- (11) Piner, R. D.; Zhu, J.; Xu, F.; Hong, S. H.; Mirkin, C. A. *Science* **1999**, 283, 661.
- (12) Krupke, R.; Hennrich, F.; Löheynes, H. V.; Kappes, M. M. *Science* **2003**, 301, 344.
- (13) Blatt, S.; Hennrich, F.; Löheynes, H. V.; Kappes, M. M.; Vijayaraghavan, A.; Krupke, R. *Nano Lett.* **2007**, 7, 1960.
- (14) Zhang, Z. B.; Liu, X. J.; Campbell, E. E. B.; Zhang, S. L. *J. Appl. Phys.* **2005**, 98, 056103.
- (15) Ranjan, N.; Vinzelberg, H.; Mertig, M. *Small* **2006**, 2, 1490.
- (16) Smith, P. A.; Nordquist, C. D.; Jackson, T. N.; Mayer, T. S.; Martin, B. R.; Mbainyo, J.; Mallouk, T. E. *Appl. Phys. Lett.* **2000**, 77, 1399.
- (17) Englander, O.; Christensen, D.; Kim, J.; Lin, L.; Morris, S. J. S. *Nano Lett.* **2005**, 5, 705.
- (18) Kong, K. H.; Deneke, C.; Schmidt, H.; Thurmer, D. J.; Ji, H. X.; Bauer, M.; Schmidt, O. G. *Appl. Phys. Lett.* **2010**, 96, 134105.

- (19) Tuukkanen, S.; Toppari, J. J.; Kuzyk, A.; Hirviniemi, L.; Hytönen, V. P.; Inhalainen, T.; Törma, P. *Nano Lett.* **2006**, *6*, 1339.
- (20) Habibi, Y.; Heim, T.; Douillard, R. *J. Polym. Sci., Part B* **2008**, *46*, 1430.
- (21) Messmore, B. W.; Hulvat, J. F.; Sone, E. D.; Stupp, S. I. *J. Am. Chem. Soc.* **2004**, *126*, 14452.
- (22) Sardone, L.; Palermo, V.; Devaux, E.; Credgington, D.; de Loos, M.; Marletta, G.; Cacialli, F.; van Esch, J.; Samori, P. *Adv. Mater.* **2006**, *18*, 1276.
- (23) Yoshio, M.; Shoji, Y.; Tochigi, Y.; Nishikawa, Y.; Kato, T. *J. Am. Chem. Soc.* **2009**, *131*, 6763.
- (24) (a) Serrano, J. L.; Sierra, T. *Coord. Chem. Rev.* **2003**, *242*, 73.
(b) Barberá, J.; Cavero, E.; Lehmann, M.; Serrano, J.-L.; Sierra, T.; Vázquez, J. T. *J. Am. Chem. Soc.* **2003**, *125*, 4527. (c) Camerel, F.; Strauch, P.; Antonietti, M.; Faul, C. F. *J. Chem.—Eur. J.* **2003**, *9*, 3764.
(d) Cavero, E.; Uriel, S.; Romero, P.; Serrano, J. L.; Giménez, R. *J. Am. Chem. Soc.* **2007**, *129*, 11608. (e) Frischmann, P. D.; Guieu, S.; Tabeshi, R.; MacLachlan, M. J. *J. Am. Chem. Soc.* **2010**, *132*, 7668.
- (25) Norman, J. G.; Renzoni, G. E.; Case, D. A. *J. Am. Chem. Soc.* **1979**, *101*, 5256.
- (26) Barral, M. C.; González-Prieto, R.; Jiménez-Aparicio, R.; Priego, J. L.; Torres, M. R.; Urbanos, F. A. *Eur. J. Inorg. Chem.* **2004**, 4491.
- (27) (a) Olea, D.; González-Prieto, R.; Priego, J. L.; Barral, M. C.; de Pablo, P. J.; Torres, M. R.; Gómez-Herrero, J.; Jiménez-Aparicio, R.; Zamora, F. *Chem. Commun.* **2007**, 1591. (b) Welte, L.; González-Prieto, R.; Olea, D.; Torres, M. R.; Priego, J. L.; Jiménez-Aparicio, R.; Gómez-Herrero, J.; Zamora, F. *ACS Nano* **2008**, *2*, 2051.
- (28) Rusjan, M.; Donnio, B.; Heinrich, B.; Cukierman, F. D.; Guillou, D. *Langmuir* **2002**, *18*, 10116.
- (29) Castro, M. A.; Roitberg, A. E.; Cukierman, F. D. *Inorg. Chem.* **2008**, *47*, 4682.
- (30) Estiú, G.; Cukierman, F. D.; Maldivi, P.; Poizat, O. *Inorg. Chem.* **1999**, *38*, 3030.
- (31) Miskowski, V. M.; Gray, H. B. *Inorg. Chem.* **1988**, *27*, 2501.
- (32) Palmans, A. R. A.; Vekemans, J. A. J. M.; Fischer, H.; Hikmet, R. A.; Meijer, E. W. *Chem.—Eur. J.* **1997**, *3*, 300.